Reexamining the role of I^3 in mass formulas via the double-difference of binding energies

Junyao Kong, Yibin Qian,* and Rui Wang

Department of Applied Physics and MIIT Key Laboratory of Semiconductor Microstructure and Quantum Sensing, Nanjing University of Science and Technology, Nanjing 210094, China

(Received 4 February 2026; revised 7 July 2026; accepted 27 August 2026; published 14 September 2026)

Conventional nuclear mass formulas, predicated on the charge independence of nucleon-nucleon (NN) interactions, generally parametrize the neutron-proton asymmetry [$I = (N - Z)/A$] using even powers or absolute values. Previously, an I^3 term was incorporated into the classical liquid drop model to examine the influence of isospin symmetry breaking (ISB) on nuclear mass. Although this term captures the ISB effect especially in the mass region of large isospin asymmetry, its directly fitted coefficient is often overshadowed by the dominant macroscopic background. This may lead to numerically entangled and physically unreasonable values, which would undermine the credibility of subsequent conclusions regarding the breaking effect. To address this issue, this paper utilizes a double-difference analysis of binding energies to extract a more physically rational coefficient for the I^3 term. Benefiting from the isospin-related terms, the coefficients of these terms all have been refined, during which the volume symmetry energy coefficient was readjusted to around -29 MeV. This is slightly lower than the typical results found in previous models. Furthermore, the ratio of surface symmetry energy coefficient to the volume symmetry energy coefficient is in the range of 1.6–1.8, which is in good agreement with the results reported in previous works. More importantly, the value of the ISB term coefficient, as expected, was refined to -3.7 ± 0.65 MeV. Although the contribution of this term to nuclear mass in the liquid drop model is small, the extracted values remain highly stable, particularly when approaching the neutron-rich region.

DOI: 10.1103/dr2g-kttx

I. INTRODUCTION

The atomic nucleus, characterized as a highly complex quantum many-body system, remains structurally enigmatic. This persists due to enduring ambiguities in the fundamental nature of the nuclear force, further compounded by the intrinsic challenges of the many-body problem. Currently, nuclear mass (or binding energy) serves as a primary observable for probing the essence of the fundamental nucleon-nucleon (NN) interaction. In addition, mass predictions for unknown nuclides are of paramount importance for various applications in fundamental physics. To this end, numerous mass models have been developed to predict nuclide masses with high precision, including the Weizsäcker-Skyrme model [1], the finite-range droplet model [2], the Hartree-Fock-Bogoliubov approach [3–5], and the Duflo-Zuker model [6]. Traditionally, predicated on the charge independence of the NN interaction, neutrons and protons are treated as two distinct charge states of the same underlying particle. In the absence of Coulomb effects, strict isospin symmetry would imply a striking correspondence between the structural properties of mirror nuclei. For instance, isobaric analog states [7,8] within the same isospin multiplet should exhibit degenerate energy levels under stringent isospin conservation—a feature observed experimentally in certain light systems [9]. Consistent with this observation, it has been conjectured that mass differences between mirror nuclei should be exclusively explained by Coulomb energy. Following this logic, terms dependent on the isospin asymmetry I in these mass models are typically expressed in even powers or absolute values to maintain symmetry. These two conjectures have been individually covered in previous studies, such as the study of charge independence in medium weight nuclei [10,11]. However, recent experimental data have revealed subtle deviations from this idealized symmetry. Experimental NN phase shifts reveal that the neutron-neutron interaction (V_{nn}) is approximately 1% stronger than the proton-proton interaction (V_{pp}), while the proton-neutron interaction (V_{pn}) exceeds the average of V_{nn} and V_{pp} by roughly 2.5% [12]. These phenomena are categorized as charge-symmetry breaking and charge-independence breaking, respectively [12]. Therefore, isospin-symmetry-breaking (ISB) effects should be explicitly incorporated into the study of nuclear structure [13–19]. In our previous work [20], we investigated these effects by introducing an I^3 term into the liquid drop formula to break the traditional even-power regulation. Nonetheless, despite these initial efforts, several issues remain. On one hand, the extracted macroscopic coefficients often lack physical rationality due to their entanglement with the dominant bulk background. On the other hand, the unconsidered microscopic effects further distort these parameters.

To overcome these limitations, an alternative strategy is required—one designed to eliminate microscopic fluctuations

*Contact author: qyibin@njust.edu.cn

 ©2026 American Physical Society

and robustly extract a physically rational I^3 coefficient. Notably, this requirement is aligned with the double-difference (DD) method recently highlighted in Refs. [21–24]. By utilizing mass differences between multiple neighboring nuclei, this method effectively cancels out microscopic effects (e.g., shell and pairing fluctuations), providing a pristine environment for extracting the isospin-symmetry breaking. Therefore, we aim to employ the DD method to extract a more physically meaningful coefficient for the I^3 term. The details of this methodology are presented in the next subsection.

The remainder of this article is organized as follows. Section II details the double-difference method and its application in extracting the I^3 term of the symmetry energy. Section III provides a comparative analysis of I^3 effects across the liquid drop model, alongside an evaluation of its contribution to $R_{ip\text{-}jn}(Z, A)$. Finally, a summary of our findings is presented in Sec. IV.

II. METHODS

Nuclear mass, or binding energy (BE), is a fundamental physical quantity in nuclear physics. Its precise measurement not only facilitates the refinement of nuclear models but also yields profound insights into NN interactions, shell evolution, and nuclear shape transitions [25]. Recently, numerous mass models have been proposed, which often exhibit significant deviations when extrapolated far from the valley of stability, despite their proximity to experimental data within known regions. Consequently, local mass relations, such as the Garvey-Kelson relations and others [26–33], remain indispensable for describing Be with high precision. Meanwhile, owing to the discrepancies in the predictions of various models in the neutron-rich region, interactions involving ISB have also garnered considerable attention, particularly in their role in characterizing symmetry energy and nuclear mass [19,34]. In this context, the I^3 term serves as a straightforward yet effective manifestation of the ISB effect within the conventional liquid drop (LD) formula,

$$\begin{aligned} B(A,Z) = {} & a_v A + a_s A^{2/3} + a_c \frac{Z^2}{A^{1/3}} + a_t \frac{(N-Z)^2}{A} \\ & + a_{\rm xc} \frac{Z^{4/3}}{A^{1/3}} + a_w \frac{|N-Z|}{A} + a_{\rm st} \frac{(N-Z)^2}{A^{4/3}} \\ & + a_3 I^3 A + a_{\rm pair} A^{-1/2} \delta_{np}. \end{aligned} \tag{1}$$

Here, $I = (N-Z)/A$, and the coefficients a_v, a_s, a_c, $a_{\rm xc}$, a_w, and $a_{\rm pair}$ correspond to the volume, surface, Coulomb, exchange Coulomb, Wigner, and pairing energy terms, respectively.

To determine these coefficients, we performed an initial global fit to the experimental binding energies from the AME table [35,36]. The results are summarized in Table I. However, directly extracting the isospin-breaking coefficient a_3 from binding energies leads to severe problems. This arises because the a_3 coefficient is obscured by the dominant macroscopic background and distorted by microscopic fluctuations, thereby compromising the physical validity of the extracted values. These issues underscore the necessity for a more refined differential approach to isolate the ISB effect. As established in Ref. [37], double-differences constitute a robust tool for investigating various correlations by canceling out common macroscopic and microscopic contributions. This methodology provides an excellent opportunity to study the correlation between the ISB effect and the mass number A while preserving physical rationality. Our analysis proceeds in two steps. First, the macroscopic contributions—specifically the volume, surface, Coulomb, exchange Coulomb, Wigner, and pairing terms—are subtracted from the experimental BE. The residual component, which represents the required symmetry energy, is denoted as $e(Z, A)$,

$$\begin{aligned} e(Z,A) = B(N,Z) - \Bigg[& a_v A + a_s A^{2/3} + a_c \frac{Z^2}{A^{1/3}} \\ & + a_{\rm xc} \frac{Z^{4/3}}{A^{1/3}} + a_w \frac{|N-Z|}{A} + a_{\rm pair} A^{-1/2} \delta_{np} \Bigg]. \end{aligned} \tag{2}$$

It is worth noting that fixing these six macroscopic parameters in Eq. (2) is not a subjective statistical manipulation intended to artificially reduce the uncertainties of the remaining symmetry energy coefficients. We acknowledge that in a standard global fit of total binding energies $B(N, Z)$, manually fixing parameters would indeed artificially narrow the error bounds. However, our methodology operates entirely within a differential space. The physical essence of the DD method is to structurally filter out the overwhelming bulk background in order to isolate the targeted localized signal. This filtering mechanism is mathematically executed by constructing a specific difference operator (DD operator). As is shown in the subsequent double-difference operations, the DD operator functions analytically as a discrete second-order derivative on the binding energy surface. This transformation inherently projects smooth macroscopic components (such as volume, surface, and Coulomb energies) into a near-null space. Attempting to treat these smooth components as free parameters within the differential space would lead to a rank-deficient Jacobian matrix, rendering the numerical optimization ill-posed. Therefore, fixing the predetermined macroscopic baseline is a strict mathematical requirement to eliminate redundant degrees of freedom, ensuring the convergence and uniqueness of the target parameters. The

TABLE I. Parameter set (scale in MeV) for the LD formula Eq. (1) by matching the AME table [35,36], including the mean value, the statistical deviation, and the relative uncertainty.

a_i	$\bar{a}_i$	σ_i	$\lvert\sigma_i/\bar{a}_i\rvert$
a_v	15.201	0.037	0.243%
a_s	−17.844	0.139	0.779%
a_c	−0.705	0.002	0.284%
a_t	−27.664	0.391	1.413%
$a_{\rm xc}$	1.504	0.126	8.377%
a_w	−46.333	4.274	9.225%
$a_{\rm st}$	48.620	1.932	3.973%
a_3	−4.61	0.942	20.433%
$a_{\rm pair}$	11.395	0.713	6.257%

TABLE II. Best-fit symmetry energy coefficients a_t, a_{st}, and a_3 (in MeV) extracted via the double-difference method [Eq. (A1)] using experimental binding energies from the AME2020 dataset. Results obtained by calculating the residual symmetry energy $e(Z, A)$ using the macroscopic coefficients from the LD model. The final row ($R_{ip\text{-}jn}$) provides the global fit integrated all step indices. Note that the statistical uncertainties of $R_{ip\text{-}jn}$ have been conservatively adjusted by $f_{\text{inflation}} \approx 2.21$ to account for the correlations induced by shared reference nuclei.

Channel	a_t (MeV)	a_{st} (MeV)	a_3 (MeV)	$\lvert\kappa_{s/v}\rvert$
$R_{1p\text{-}2n}$	-30.10 ± 2.09	51.15 ± 7.11	-2.31 ± 1.52	1.70 ± 0.26
$R_{2p\text{-}1n}$	-30.38 ± 2.14	52.48 ± 7.27	-2.80 ± 1.55	1.73 ± 0.27
$R_{2p\text{-}2n}$	-29.96 ± 1.15	51.64 ± 3.91	-3.49 ± 0.85	1.72 ± 0.15
$R_{2p\text{-}3n}$	-29.66 ± 0.86	51.01 ± 2.92	-3.89 ± 0.65	1.72 ± 0.11
$R_{3p\text{-}2n}$	-29.88 ± 0.88	51.79 ± 2.98	-3.81 ± 0.66	1.73 ± 0.11
$R_{3p\text{-}3n}$	-29.19 ± 0.65	49.02 ± 2.20	-3.89 ± 0.51	1.68 ± 0.08
Global	-29.61 ± 0.88	50.55 ± 3.00	-3.72 ± 0.65	1.71 ± 0.11

subsequent stage involves calculating the double-difference of $e(Z, A)$, denoted by $R_{ip\text{-}jn}(Z, A)$. Following the algebraic structure of $\delta V_{ip\text{-}jn}$, we define $R_{ip\text{-}jn}(Z, A)$ as follows,

$$R_{ip\text{-}jn}(Z, A) = e(Z, A) + e(Z - i, A - i - j) - e(Z, A - j) - e(Z - i, A - i). \quad (3)$$

In this study, the step indices are assigned as $(i, j) = (1, 2), (2, 1), (2, 2), (2, 3), (3, 2)$, and (3,3). By parametrizing the symmetry energy as $e(Z, A) = (a_t + a_{st}A^{-1/3})I^2A + a_3I^3A$, we derive the full analytical expression for $R_{ip\text{-}jn}(Z, A)$. As shown in Eq. (A1), the terms are organized to highlight their dependence on the isospin asymmetry I.

Following the definition of the double-difference operator, it is imperative to establish a rigorous error propagation framework to ensure the physical reliability of the extracted coefficients. In our analysis, the uncertainties are systematically propagated directly from the intrinsic experimental errors of the binding energies (σ_{exp}). For the residual component $e(Z, A)$, the corresponding uncertainty σ_e is calculated by coupling the pure experimental error with the statistical fluctuation transferred from the macroscopic baseline. This is formulated as $\sigma_e = \sqrt{\sigma_{\text{exp}}^2 + \sigma_{\text{macro}}^2}$, where σ_{macro}^2 is derived from the covariance matrix of the fixed macroscopic parameters via the corresponding Jacobian matrix. Subsequently, this well-defined statistical uncertainty is rigorously propagated into the differential space. For each specific (i, j) channel, the uncertainty of the double-difference observable, denoted as σ_R, is strictly determined by the root sum square of the propagated errors from the four constituent nuclei: $\sigma_R = \sqrt{\sigma_1^2 + \sigma_2^2 + \sigma_3^2 + \sigma_4^2}$. This step guarantees that the localized differential observables are appropriately weighted by their absolute experimental precision prior to any parameter extraction. Finally, when performing the global multidimensional optimization across all extracted channels, one must account for the statistical correlations induced by the shared use of reference nuclei in the binding energy surface. To rigorously penalize the final error bounds and prevent any artificial underestimation of the uncertainties, an inflation factor $f_{\text{inflation}}$ is adopted based on the mean correlation coefficient of the extracted channels. By applying this inflation factor, the physical errors of the targeted isospin-breaking parameters are comprehensively constrained and robustly shielded from statistical artifacts.

III. RESULTS AND DISCUSSION

Using the proposed methodology, $R_{ip\text{-}jn}(Z, A)$ was calculated for nuclei with high-precision experimental data available in the AME atomic mass evaluation [35,36]. Equation (A1) was subsequently employed to extract the best-fit coefficients a_t, a_{st}, and a_3. The resulting parameters for various (i, j) step indices—specifically (1, 2), (2, 1), (2, 2), (2, 3), (3, 2), and (3,3)—are summarized in Table II and illustrated in Fig. 1. As depicted in Fig. 1, $R_{ip\text{-}jn}$ exhibits a robust correlation with the mass number A, characterized by an overall monotonic decrease that asymptotically approaches a constant value in the heavy-mass region. Compared to prior investigations [21], the explicit integration of the I^3 term reveals a pronounced parity effect, which

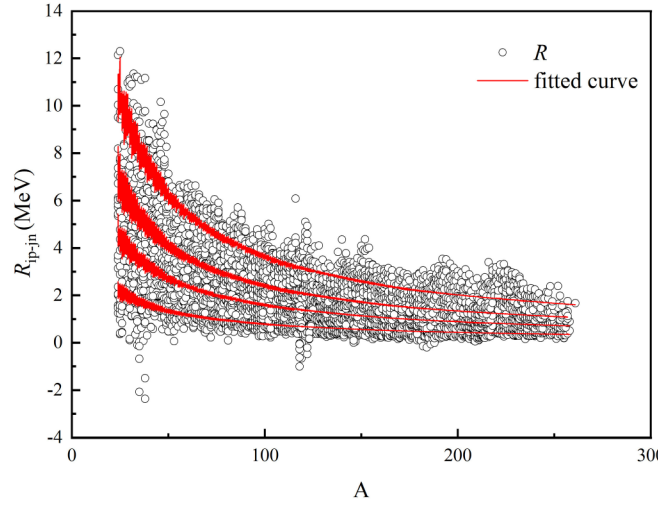

FIG. 1. The results of $R_{ip\text{-}jn}(Z, A)$ with the changing trend of A for $(i, j) = (1, 2), (2, 1), (2, 2), (2, 3), (3, 2)$ and (3,3), respectively. The black dots represent the calculation results of the experimental values and the red lines represent the fitting curve of Eq. (A1). Note that the results of (1,2) and (2,1) [similar to (2,3) and (3,2)] shown in the figure almost overlapped.

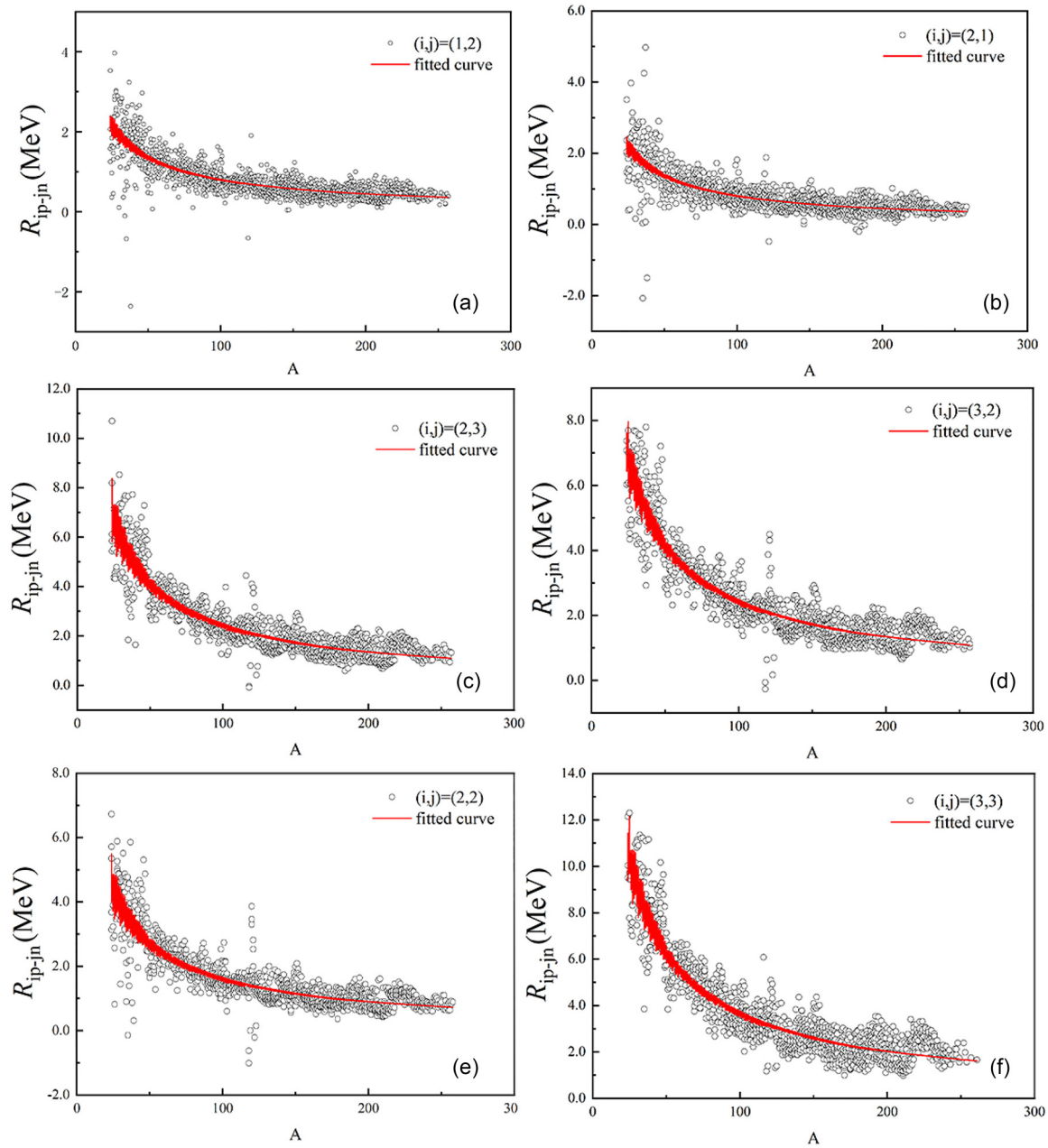

FIG. 2. The double-difference results $R_{ip\text{-}jn}(Z, A)$ as a function of the mass number A, displayed in separate panels for various step indices (i, j): (a) (1,2); (b) (2,1); (c) (2,3); (d) (3,2); (e) (2,2); and (f) (3,3). The open circles denote the experimental values derived from the AME2020 dataset, while the solid red lines represent the corresponding theoretical fitting curves based on Eq. (A1).

facilitates superior alignment between the theoretical fit (red lines) and experimental observations (black dots). Notably, the results for symmetric pairs such as (1,2) and (2,1), as well as (2,3) and (3,2), exhibit significant overlapping, further validating the consistency of the extraction procedure. To provide a clearer visualization of the fitting performance, the overlaid trends in Fig. 1 are decomposed into separate panels according to their specific (i, j) indices, as illustrated in Fig. 2. Furthermore, across these separate panels, a localized peak is consistently observed around $A \approx 120$. This feature is attributed to the inclusion of experimental data near magic numbers. Although the double-difference method effectively neutralizes a significant portion of the macroscopic and microscopic fluctuations, residual shell effects persist, particularly in the vicinity of $A \approx 120$ where magic nuclei cluster. Moreover, this region is known for complex structural phenomena, such as shape coexistence, which may contribute to these localized deviations and warrant further investigation [38].

The extracted parameters are summarized in Table II, where $\kappa_{s/v} = a_{\rm st}/a_t$ represents the surface-to-volume ratio of the symmetry energy. Based on the LD model, this yields $a_t = -29.61 \pm 0.88$ MeV, $a_{\rm st} = 50.55 \pm 3.00$ MeV, and $a_3 = -3.72 \pm 0.65$ MeV (with $\kappa_{s/v} = 1.71 \pm 0.11$). Compared

with the earlier estimations in Ref. [21], the uncertainties of extracted parameters in this work are larger. This is primarily attributed to the present treatment. Furthermore, while the combined multidimensional fit yields the most robust parameter extraction, examining the behavior of the individual (i, j) channels provides valuable physical insights. As observed in Table II, the extracted coefficients (a_t, $a_{\rm st}$, and a_3) exhibit slight variations depending on the specific step indices. Rather than indicating statistical instability, these variations are a natural consequence of the DD approach acting as a localized discrete filter on the binding energy surface. The nuclear chart is replete with complex, highly localized structural phenomena, such as subshell closures and shape coexistence. If a specific (i, j) difference window traverses a boundary of abrupt structural evolution, the structural cancellation within that localized region may be inherently imperfect. Consequently, these residual localized microscopic fluctuations propagate into the fitting procedure, manifesting as the slight channel-dependent deviations observed in the extracted macroscopic coefficients.

To obtain the most robust and universal macroscopic parameters, it is essential to mitigate the potential structural bias introduced by any single localized sampling window. The final row in Table II presents the global fit integrating all considered (i, j) configurations. Rather than acting as a simple arithmetic average, this global integration represents a comprehensive multidimensional optimization over the extended parameter space (Z, A, i, j). By treating the step indices i and j as independent variables, the fitting procedure synthesizes complementary physical information from distinct configurational directions on the binding energy surface. This approach systematically neutralizes the aforementioned localized structural fluctuations while strictly preserving the unique physical constraints provided by each specific double-difference path. Consequently, the multidimensional fit yields highly stabilized macroscopic parameters and guarantees a physically decoupled, robust extraction of the a_3 coefficient.

To quantitatively evaluate the reliability of the extracted coefficients, we strictly executed the error propagation framework formulated in Sec. II. As listed in Table II, the initial uncertainties for individual (i, j) channels are fundamentally driven by the absolute experimental precision ($\sigma_{\rm exp}$) coupled with the statistical fluctuations propagated from the macroscopic baseline. This rigorous tracking through the differential operator ensures that the fitting weights are strictly grounded in measurable physical uncertainties rather than arbitrary statistical assumptions.

However, while the multidimensional optimization over the extended parameter space (Z, A, i, j) significantly stabilizes the parameter extraction, the statistical correlations introduced by the shared use of reference nuclei (Z, A) across the six distinct (i, j) paths must be rigorously addressed. As shown in Fig. 3, evaluating the correlation matrix of the extracted DD channels reveals an average off-diagonal correlation coefficient of $\overline{\rho} \approx 0.78$. To rigorously penalize the final error bounds and prevent any artificial underestimation of the uncertainties, a variance inflation factor (VIF) [39–42] is adopted. For a system of M integrated channels, the VIF is

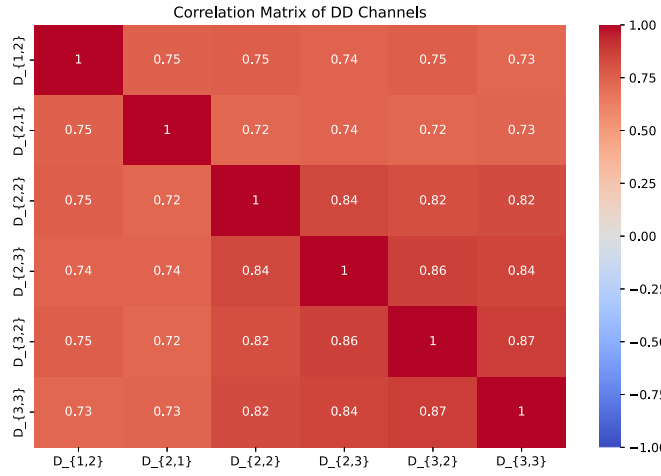

FIG. 3. The correlation matrix for the extracted double-difference (DD) channels. In this heatmap, each channel denoted as $D_{\{i,j\}}$ on the axes explicitly represents the corresponding calculated double-difference quantity $R_{ip\text{-}jn}(Z, A)$ for a given set of step indices (i, j). The off-diagonal elements indicate the correlation coefficients between these distinct $R_{ip\text{-}jn}$ observables.

theoretically defined as

$$\mathrm{VIF} = 1 + (M - 1)\bar{\rho}. \tag{4}$$

Given that the reported parameter uncertainties correspond to the standard errors (the square root of the variance), the actual scaling factor applied to our error bars is

$$f_{\rm inflation} = \sqrt{\mathrm{VIF}} = \sqrt{1 + (M - 1)\bar{\rho}}. \tag{5}$$

In our specific case with $M = 6$, the theoretical VIF is approximately 4.89, which yields an uncertainty inflation factor of $f_{\rm inflation} \approx 2.21$. It is crucial to emphasize that the uncertainties reported for the global fit ($R_{ip\text{-}jn}$) in the final row of Table II have already been fully penalized by this factor. Remarkably, even with this rigorous statistical penalty applied to the propagated experimental errors, the extraction of the a_3 parameter remains robustly constrained. This quantitatively confirms that the enhanced physical precision intrinsically originates from the background-filtering capability of the DD approach, securely decoupled from statistical artifacts.

These results are consistent with existing literature. Most notably, after applying the rigorous statistical penalty, the relative uncertainty of the a_3 parameter is robustly evaluated at approximately 17.5% ($a_3 = -3.72 \pm 0.65$ MeV). While this represents only a slight reduction from the initial 20.4% observed in the standard global fit, this conservative error bound is precisely the core physical advantage of our approach. To explicitly demonstrate that our DD methodology does not artificially manipulate or inappropriately reduce statistical uncertainties, we compare it with an alternative approach: directly fitting the residual symmetry energy $e(Z, A)$ while rigidly fixing the six macroscopic parameters, completely omitting the propagation of underlying experimental and baseline errors. The detailed results of this alternative test are provided as Set (i) in Table III of the Appendix. As shown in Set (i) of Table III, this rigid fit without error propagation leads

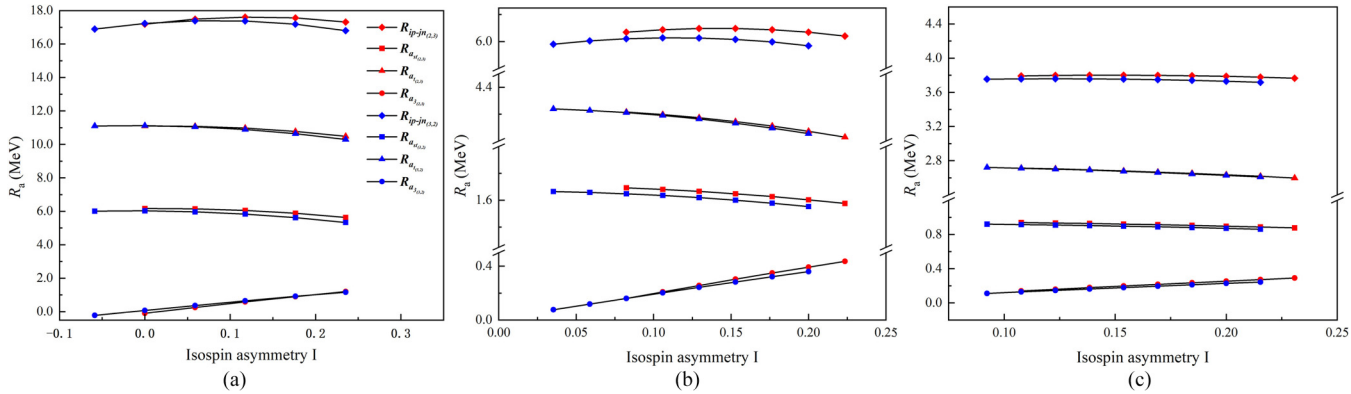

FIG. 4. Evolution of the decomposed double-difference components R_{a_i} as a function of the isospin asymmetry I for fixed mass numbers (a) $A = 34$, (b) $A = 85$, and (c) $A = 130$. The circles (R_{a_3}), squares ($R_{a_{\rm st}}$), triangles (R_{a_t}), and diamonds ($R_{ip\text{-}jn}$) represent the individual double-difference contributions and the total value, respectively.

to an unphysically extreme reduction in the uncertainties of the dominant lower-order terms ($\sigma_t = 0.080$ MeV and $\sigma_{\rm st} = 0.396$ MeV). Furthermore, without the filtering mechanism of the DD operator, the uncanceled microscopic fluctuations are forcibly absorbed by the higher-order a_3 term, severely compromising its physical purity. In contrast, Set (ii) demonstrates the results of our DD method, which intrinsically incorporates the rigorous error propagation framework. It is crucial to note that the uncertainties for the base symmetry terms extracted via the DD method ($\sigma_t = 0.88$ MeV, $\sigma_{\rm st} = 3.00$ MeV in the global fit) are notably larger and statistically healthier than those in Set (i). By acting as a discrete derivative, the DD operator physically strips away the macroscopic background and localized microscopic noise prior to parameter extraction. Consequently, the penalized uncertainty of the I^3 coefficient ($\sigma_3 = 0.65$ MeV, $\approx$17.5%) represents a genuine, physics-driven isolation of the ISB effect. This physically rational extraction is completely distinct from the artificial statistical illusions seen in direct constrained fits without proper error tracking.

Alongside the stabilization of the I^3 term, the central values of the extracted parameters exhibit a significant physical improvement over the standard nine-parameter global fit presented in Table I. In that standard global fit, the volume symmetry energy coefficient a_t drops to an unphysically low magnitude of approximately -27.6 MeV. This deviation from contemporary consensus is symptomatic of severe parameter entanglement between the ISB effect and the dominant macroscopic background. In contrast, the a_t extracted via the DD method effectively rectifies this distortion, robustly converging to approximately -29 MeV. This converged value also provides a crucial physical correction to older analyses utilizing a standard second-order symmetry energy formula (omitting the I^3 term), which typically yielded an overestimated magnitude for a_t of approximately -31 MeV. In those traditional quadratic models, the I^2 term was forced to absorb higher-order isospin-breaking effects to minimize global fitting residuals, artificially inflating the bulk symmetry energy penalty. Concurrently, the a_3 coefficient is naturally attenuated to -3.72 MeV, correcting the artificially inflated magnitude of -4.61 MeV extracted from the standard global fit. By explicitly parametrizing the I^3 term through the DD method, we successfully separate these higher-order contributions from the macroscopic baseline. This decoupling prevents the artificial inflation of the ISB effect, allowing the magnitude of a_t to relax toward a value more consistent with the symmetry energy of nuclear matter at saturation density ρ_0, while providing a physically more reasonable and structurally isolated constraint on the high-order isospin-breaking effect. This reduction in the magnitude of a_t (relative to standard quadratic models), coupled with the identical negative signs of a_t and a_3, suggests that, while the base symmetry energy is weaker than previously estimated, the total symmetry energy penalty exhibits a "stiffening" trend as the isospin asymmetry I increases. The relationship between individual symmetry energy components and isospin asymmetry (I) is further analyzed in Fig. 4 for mass numbers $A = 34$, 85, and 130, selected for their generalizability across distinct mass regions and robust experimental data.

As illustrated in Fig. 4, for all selected mass numbers, the a_3 contribution increases monotonically with isospin asymmetry. Consequently, as $A \to \infty$, the contribution of the ISB effect—encapsulated by the a_3 term—is expected to grow progressively with increasing isospin asymmetry, thereby maintaining a non-negligible role in the nuclear equation of state. Moreover, the sensitivity of the symmetry energy terms to I intensifies with increasing mass number. This trend reflects a model dependence: while the LD model describes macroscopic average properties, the a_3 term appears stable across varying asymmetries. This finding reinforces the role of the ISB effect as an integral part of understanding highly asymmetric nuclear matter. To complement the mass-number dependence, Fig. 5 illustrates the composition of total $R(Z, A)$ from its individual terms ($R_{a_{\rm st}}$, R_{a_t}, and R_{a_3}) at a fixed asymmetry of $I = 0.2$. The results indicate that the growth of total $R(Z, A)$ with A is primarily governed by the dominant volume term (a_t), whereas the relative contribution of the slower-growing surface term ($a_{\rm st}$) progressively diminishes. In addition, the contribution of the a_3 term is relatively stable, remaining around 5% and gradually increasing as A increases. The persistent influence of this term induces a discernible departure from the standard quadratic dependence of the

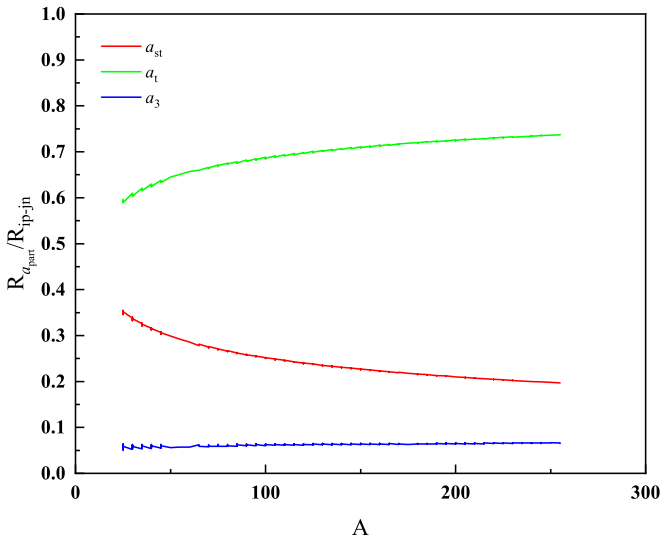

FIG. 5. Decomposition of $R_{ip\text{-}jn}$ into the contributions from $R_{a_{st}}$, R_{a_t}, and R_{a_3} via $R_{a_{part}}/R_{ip\text{-}jn}$ at a fixed isospin asymmetry of $I = 0.2$. The theoretical curves are calculated based on Eq. (A1), utilizing the global fit coefficients from the final row of Table II, which integrates all considered (i, j) step configurations. The red, green, and blue lines represent the a_{st}, a_t, and a_3 terms, respectively.

symmetry energy on I. Specifically, the inclusion of the I^3 term generates a nonlinear correction, resulting in a more rapid growth trajectory of the symmetry energy compared to standard second-order predictions.

This stiffening effect, resulting from the combined contribution of a_t and a_3, impacts the nuclear equation of state (EOS). Traditional quadratic models overestimate a_t and underestimate the symmetry energy gradient at high I, potentially leading to inaccurate descriptions of neutron-rich matter. A stiffer symmetry energy at high I indicates increased symmetry pressure, which influences the mass-radius relationship of neutron stars and the threshold for the direct Urca process in stellar cooling. Our results, characterized by $a_t \approx 29$ MeV and the a_3 term, provide constraints for extrapolating terrestrial nuclear data to neutron star cores. Furthermore, the persistent a_3 coefficient suggests that higher-order isospin-breaking effects must be explicitly incorporated into future developments of the nuclear EOS.

IV. SUMMARY

In summary, the I^3 term is essential for characterizing isospin-breaking effects within the LD formula. By applying the DD method to the AME dataset, we have refined the coefficients of symmetry-energy-related terms. Our analysis leads to three primary conclusions. First, the I^3 term coefficient is stabilized through the DD method, which mitigates localized microscopic fluctuations such as shell and pairing effects, thereby providing a physically cleaner isolation of macroscopic trends. This confirms the significance of isospin-symmetry-breaking effects in nuclear mass models. Second, the inclusion of the I^3 term facilitates a robust convergence of the volume symmetry energy coefficient a_t. Our analysis yields an a_t value of approximately -29 MeV, which is consistent across the LD framework. This explicit parametrization separates high-order isospin-breaking contributions from the standard quadratic term, allowing a_t to relax toward a value more representative of the symmetry energy at saturation density ρ_0. Consequently, this provides a more stable estimate for constraining the nuclear EOS. Finally, we find a "stiffening" effect in the symmetry energy. The synergistic contribution of a_t and a_3 leads to a more rapid growth in symmetry energy at high isospin asymmetries compared to standard second-order predictions. This persistent ISB effect remains a stable and indispensable component, maintaining a contribution that increases with the mass number A. Overall, these results underscore the role of the I^3 term in accurately characterizing the EOS of neutron-rich systems, with implications for the structural properties and cooling mechanisms of neutron stars.

TABLE III. Best-fit symmetry energy coefficients a_t, a_{st}, and a_3 (in MeV) and their statistical uncertainties. Set (i) is obtained by a direct fit to the residual symmetry energy $e(Z, A)$ with six macroscopic parameters fixed to the values from Table I, completely omitting the propagation of underlying experimental and baseline errors. Set (ii) results from the DD method, which intrinsically incorporates the rigorous error propagation framework described in Sec. II.

	Set (i)			Set (ii)		
a_i	$\bar{a}_i$	σ_i	$\lvert\sigma_i/\bar{a}_i\rvert$	$\bar{a}_i$	σ_i	$\lvert\sigma_i/\bar{a}_i\rvert$
a_t	−28.632	0.080	0.279%	−29.61	0.88	2.00%
a_{st}	52.200	0.396	0.759%	50.55	3.00	5.93%
a_3	−3.476	0.283	8.142%	−3.72	0.65	17.47%

ACKNOWLEDGMENT

This work is supported by the National Natural Science Foundation of China (Grants No. 12075121 and No. 12675157).

DATA AVAILABILITY

The data that support the findings of this article are not publicly available upon publication because it is not technically feasible and/or the cost of preparing, depositing, and hosting the data would be prohibitive within the terms of this research project. The data are available from the authors upon reasonable request.

APPENDIX

In this Appendix, we provide a detailed derivation of $R_{ip\text{-}jn}$ based on the double-difference method. This supplement serves to clarify the formulation presented in Secs. II and III, ensuring a transparent understanding of the extraction process. Furthermore, to support the physical discussion in the main text, we also present the detailed results of an alternative fitting procedure in Table III. In this comparative test, the symmetry energy coefficients are extracted via a direct fit while rigidly fixing the six macroscopic baseline parameters to the

values listed in Table I. The detailed derivation of $R_{ip\text{-}jn}$ is as follows:

$$
\begin{aligned}
R_{ip\text{-}jn}(Z,A) = a_t &\left\{ -\frac{j^2}{A-j} + \frac{(i-j)^2}{A-i-j} - \frac{i^2}{A-i} + \left[\frac{-1}{A-j} + \frac{1}{A-i-j} + \frac{1}{A} - \frac{1}{A-i} \right] I^2A^2 \right. \\
&\left. + \left[\frac{2i-2j}{A-i-j} - \frac{2i}{A-i} + \frac{2j}{A-j} \right] IA \right\} + a_{\mathrm{st}} \left\{ \left[\frac{1}{(A-j)^{4/3}} - \frac{1}{(A-i-j)^{4/3}} - \frac{1}{A^{4/3}} + \frac{1}{(A-i)^{4/3}} \right] I^2A^2 \right. \\
&\left. + \left[-\frac{2i-2j}{(A-i-j)^{4/3}} + \frac{2i}{(A-i)^{4/3}} - \frac{2j}{(A-j)^{4/3}} \right] IA + \frac{j^2}{(A-j)^{4/3}} - \frac{(i-j)^2}{(A-i-j)^{4/3}} + \frac{i^2}{(A-i)^{4/3}} \right\} \\
&+ a_3 \left\{ -\frac{i^3}{(A-i)^2} + \frac{(i-j)^3}{(A-i-j)^2} + \frac{j^3}{(A-j)^2} + \left[-\frac{3i^2}{(A-i)^2} + \frac{3(i-j)^2}{(A-i-j)^2} - \frac{3j^2}{(A-j)^2} + \right] IA \right. \\
&\left. + \left[-\frac{3i}{(A-i)^2} + \frac{3i-3j}{(A-i-j)^2} + \frac{3j}{(A-j)^2} \right] I^2A^2 + \left[\frac{1}{A^2} - \frac{1}{(A-i)^2} - \frac{1}{(A-j)^2} + \frac{1}{(A-i-j)^2} \right] I^3A^3 \right\}.
\end{aligned}
\tag{A1}
$$

[1] Z. Y. Liang, J. H. Liu, M. Liu, and N. Wang, Study on ground state properties of nuclei with Weizsäcker-Skyrme nuclear mass formula, Nucl. Phys. Rev. **28**, 262 (2011).

[2] P. Möller, A. J. Sierk, T. Ichikawa, and H. Sagawa, Nuclear ground-state masses and deformations: FRDM(2012), At. Data Nucl. Data Tables **109-110**, 1 (2016).

[3] X. W. Xia, Y. Lim, P. W. Zhao, H. Z. Liang, X. Y. Qu, Y. Chen, H. Liu, L. F. Zhang, S. Q. Zhang, Y. Kim, and J. Meng, The limits of the nuclear landscape explored by the relativistic continuum Hartree–Bogoliubov theory, At. Data Nucl. Data Tables **121-122**, 1 (2018).

[4] S. Goriely, S. Hilaire, M. Girod, and S. Péru, First Gogny-Hartree-Fock-Bogoliubov nuclear mass model, Phys. Rev. Lett. **102**, 242501 (2009).

[5] M. Samyn, S. Goriely, P.-H. Heenen, J. M. Pearson, and F. Tondeur, A Hartree–Fock–Bogoliubov mass formula, Nucl. Phys. A **700**, 142 (2002).

[6] J. Duflo and A. P. Zuker, Microscopic mass formulas, Phys. Rev. C **52**, R23 (1995).

[7] G. A. Jones, Isobaric analogue states in nuclei, Phys. Bull. **22**, 137 (1971).

[8] P. Danielewicz and J. Lee, Symmetry energy II: Isobaric analog states, Nucl. Phys. A **922**, 1 (2014).

[9] M. W. Kirson, Mutual influence of terms in a semi-empirical mass formula, Nucl. Phys. A **798**, 29 (2008).

[10] J. D. Anderson and C. Wong, Evidence for charge independence in medium weight nuclei, Phys. Rev. Lett. **7**, 250 (1961).

[11] M. Bentley and S. Lenzi, Coulomb energy differences between high-spin states in isobaric multiplets, Prog. Part. Nucl. Phys. **59**, 497 (2007).

[12] R. Machleidt and D. Entem, Chiral effective field theory and nuclear forces, Phys. Rep. **503**, 1 (2011).

[13] S. M. Lenzi, A. Poves, and A. O. Macchiavelli, Isospin symmetry breaking in the mirror pair ^{73}Sr-^{73}Br, Phys. Rev. C **102**, 031302(R) (2020).

[14] H. Sagawa, T. Naito, X. Roca-Maza, and T. Hatsuda, QCD-based charge symmetry breaking interaction and the Okamoto-Nolen-Schiffer anomaly, Phys. Rev. C **109**, L011302 (2024).

[15] J. W. Negele, The ^{41}Sc-^{41}Ca Coulomb energy difference, Nucl. Phys. A **165**, 305 (1971).

[16] J. M. Dong, Y. H. Zhang, W. Zuo, J. Z. Gu, L. J. Wang, and Y. Sun, Generalized isobaric multiplet mass equation and its application to the Nolen-Schiffer anomaly, Phys. Rev. C **97**, 021301(R) (2018).

[17] Z.-T. Xia and W. Zuo, Isospin-symmetry breaking effects on the strange electric and magnetic form factors of the nucleon, Phys. Rev. C **78**, 015209 (2008).

[18] H. H. Li, Q. Yuan, J. G. Li, M. R. Xie, S. Zhang, Y. H. Zhang, X. X. Xu, N. Michel, F. R. Xu, and W. Zuo, Investigation of isospin-symmetry breaking in mirror energy difference and nuclear mass with *ab initio* calculations, Phys. Rev. C **107**, 014302 (2023).

[19] X. Roca-Maza, G. Colò, and H. Sagawa, Nuclear symmetry energy and the breaking of the isospin symmetry: How do they reconcile with each other? Phys. Rev. Lett. **120**, 202501 (2018).

[20] J. Y. Kong and Y. B. Qian, Including an I^3 term in the liquid drop model: Isospin breaking of the NN interaction in the nuclear mass formula, Phys. Rev. C **110**, 054303 (2024).

[21] H. Jiang, G. J. Fu, Y. M. Zhao, and A. Arima, Volume and surface symmetry energy coefficients, Phys. Rev. C **85**, 024301 (2012).

[22] H. Jiang, N. Wang, L.-W. Chen, Y. M. Zhao, and A. Arima, Model dependence of the I^4 term in the symmetry energy for finite nuclei, Phys. Rev. C **91**, 054302 (2015).

[23] H. Jiang, M. Bao, L.-W. Chen, Y. M. Zhao, and A. Arima, I^4 dependence in nuclear symmetry energy, Phys. Rev. C **90**, 064303 (2014).

[24] H. Jiang, Y. Y. Cheng, N. Wang, L.-W. Chen, Y. M. Zhao, and A. Arima, Robustness of the I^4 symmetry energy coefficient, Phys. Rev. C **94**, 064301 (2016).

[25] D. Lunney, J. M. Pearson, and C. Thibault, Recent trends in the determination of nuclear masses, Rev. Mod. Phys. **75**, 1021 (2003).

[26] G. T. Garvey and I. Kelson, New nuclidic mass relationship, Phys. Rev. Lett. **16**, 197 (1966).

[27] G. T. Garvey, W. J. Gerace, R. L. Jaffe, I. Talmi, and I. Kelson, Set of nuclear-mass relations and a resultant mass table, Rev. Mod. Phys. **41**, S1 (1969).

[28] J. Jänecke and H. Behrens, Nuclidic mass relationships and mass equations, Phys. Rev. C **9**, 1276 (1974).

[29] J. Jänecke, Updated mass predictions from the Garvey-Kelson mass relations, At. Data Nucl. Data Tables **17**, 455 (1976).

[30] Z. He, M. Bao, Y. M. Zhao, and A. Arima, New features of the Garvey-Kelson mass relations, Phys. Rev. C **87**, 057304 (2013).

[31] J. Tian, N. Wang, C. Li, and J. Li, Improved Kelson-Garvey mass relations for proton-rich nuclei, Phys. Rev. C **87**, 014313 (2013).

[32] B. A. Brown, R. R. C. Clement, H. Schatz, A. Volya, and W. A. Richter, Proton drip-line calculations and the *rp* process, Phys. Rev. C **65**, 045802 (2002).

[33] C. Ma, Y. Y. Zong, S. Q. Zhang, J. Li, K. Wang, Y. M. Zhao, and A. Arima, Mass relations of mirror nuclei in terms of Coulomb energies based on relativistic continuum Hartree-Bogoliubov calculations, Phys. Rev. C **103**, 054326 (2021).

[34] P. Bączyk, J. Dobaczewski, M. Konieczka, W. Satuła, T. Nakatsukasa, and K. Sato, Isospin-symmetry breaking in masses of $N \simeq Z$ nuclei, Phys. Lett. B **778**, 178 (2018).

[35] G. Audi, M. Wang, A. Wapstra, F. Kondev, M. MacCormick, and X. Xu, The 2012 atomic mass evaluation and the mass tables, Nucl. Data Sheets **120**, 1 (2014).

[36] M. Wang, G. Audi, F. G. Kondev, W. J. Huang, S. Naimi, and X. Xu, The AME2016 atomic mass evaluation (II). Tables, graphs and references, Chin. Phys. C **41**, 030003 (2017).

[37] D. Brenner, C. Wesselborg, R. Casten, D. Warner, and J.-Y. Zhang, Empirical p-n interactions: Global trends, configuration sensitivity and $N=Z$ enhancements, Phys. Lett. B **243**, 1 (1990).

[38] K. Heyde and J. L. Wood, Shape coexistence in atomic nuclei, Rev. Mod. Phys. **83**, 1467 (2011).

[39] L. Kish, *Survey Sampling* (John Wiley & Sons, New York, 1965).

[40] K.-Y. Liang and S. L. Zeger, Longitudinal data analysis using generalized linear models, Biometrika **73**, 13 (1986).

[41] A. J. Scott and D. Holt, The effect of two-stage sampling on ordinary least squares methods, J. Am. Stat. Assoc. **77**, 848 (1982).

[42] S. Killip, Z. Mahfoud, and K. Pearce, What is an intracluster correlation coefficient? Crucial concepts for primary care researchers, Ann. Fam. Med. **2**, 204 (2004).